metals

MDPI

Article

Study on High-Temperature Low-Cycle Fatigue Behavior of the FGH96 Superalloy Based on Internal Stress Division

Zhengguang Li, Haiqin Qin *, Kejun Xu, Zhenbo Xie, Pengcheng Ji and Mingming Jia

Qingdao Campus, Naval Aviation University, Qingdao 266041, China
* Correspondence: xiao_qin_1981@163.com

Abstract: In order to deeply explore the high-temperature cyclic characteristics of the FGH96 superalloy under different strain amplitudes, the high-temperature low-cycle fatigue behavior of the FGH96 superalloy was analyzed from the perspective of internal stress evolution. Four sets of strain amplitude (0.5%, 0.6%, 0.8%, and 1.2%) controlled high-temperature low-cycle fatigue tests were carried out on the FGH96 superalloy at 550 °C, and the internal stress was divided into back stress and effective stress through the cyclic stress-strain curves. The results show that the cyclic softening/hardening characteristics of the FGH96 superalloy under different strain amplitudes are closely related to the evolution of internal stress. The strain amplitude has a significant effect on the back stress of the FGH96 superalloy but has little effect on effective stress. At low strain amplitudes (0.5% and 0.6%), the back stress evolution rate of the FGH96 superalloy is lower than effective stress, and the material mainly exhibits cyclic softening. At high strain amplitudes (0.8% and 1.2%), the back stress evolution rate of the FGH96 superalloy is significantly higher than effective stress, and the material exhibits cyclic hardening. The combined effect of back stress and effective stress is the main reason for the different low-cycle fatigue behaviors of the FGH96 superalloy under different strain amplitudes.

Keywords: high-temperature low-cycle fatigue; the FGH96 superalloy; internal stress evolution; cyclic softening/hardening

check for updates

Citation: Li, Z.; Qin, H.; Xu, K.; Xie, Z.; Ji, P.; Jia, M. Study on High-Temperature Low-Cycle Fatigue Behavior of the FGH96 Superalloy Based on Internal Stress Division. *Metals* **2023**, *13*, 1705. https://doi.org/10.3390/met13101705

Academic Editor: Lakhdar Taleb

Received: 9 September 2023
Revised: 30 September 2023
Accepted: 6 October 2023
Published: 7 October 2023

1. Introduction

With the rapid development of aviation technology, the requirements for the thrust-to-weight ratio, turbine speed, and other performance of aero-engines are constantly increasing. As a result, key components of aero-engines, such as turbine disks, are subjected to more severe and complex load conditions [1,2]. In order to meet the increasingly complex working conditions of aero-engine turbine disks and other core components, powder metallurgy superalloy materials have risen to the occasion. The FGH96 superalloy is representative of the second generation of damage-resistant powder superalloys [3,4]. Compared with the first-generation powder metallurgy superalloy, the FGH96 superalloy appropriately reduces the strength level of the alloy, improves crack growth resistance and creep resistance, has a higher yield strength, and has excellent high temperature damage tolerance characteristics. As the current preferred material for aero-engine hot-end components, the FGH96 superalloy is now widely used in aero-engine turbine disks [5,6].

In actual work, aero-engines need to continuously start, accelerate, decelerate, brake, and stop. The turbine system is subject to complex cyclic loads, leading to the initiation and expansion of structural cracks, thereby limiting the service life of the aero-engine and threatening flight safety. Research shows that the damage mechanisms of turbine disks include low-cycle fatigue, high-cycle fatigue, creep, high-temperature corrosion, etc. Among them, high-temperature, low-cycle fatigue is one of the main failure modes that limit the use of turbine disks [7]. Therefore, understanding the mechanical behavior of the FGH96 superalloy under high temperature and low-cycle fatigue loading is of great significance for the life design and structural integrity assessment of aero-engines.

Internal stress is the macroscopic performance of the internal microstructure of the material, and the macroscopic deformation mechanism of the material can be analyzed by using the method of internal stress division [8]. In order to explain the deformation characteristics of crystal materials under cyclic loading, Cottrell [9] first divided the internal stress into back stress and effective stress. Among them, the back stress microscopically represents the long-range force in dislocation motion, macroscopically reflects the translation of the yield surface in the macroscopic stress space, and represents the kinematic hardening of the material. Effective stress microscopically represents the short-range force of dislocation movement, that is, the critical condition required for dislocation movement. Macroscopically, it reflects the expansion or contraction of the yield surface and represents the isotropic hardening law of the material [8–10]. Based on Cottrell's internal stress division theory, scholars have carried out a large amount of research work, revealing the connection between internal stress and material microstructure changes [10–14] and explaining the influence of internal stress components on material cycle characteristics [10–15], which proved the effectiveness of the theory in studying the macroscopic mechanical properties of materials under cyclic loading. At the same time, as two important parameters of the constitutive model, the establishment of corresponding constitutive models and the acquisition of relevant parameters based on the evolution characteristics of back stress and effective stress of different materials can greatly increase the accuracy of material modeling [16–20].

Compared with traditional experimental analysis, internal stress has a clearer physical meaning and can also reflect the connection between the material's microstructure and macroscopic deformation [8,10]. However, there are few studies on the application of internal stress to the low-cycle fatigue behavior of powder superalloys, and even fewer studies on the application of internal stress to the FGH96 superalloy in the turbine disk service environment. In previous work, our research group only analyzed the cyclic softening/hardening phenomenon of the FGH96 superalloy from the perspective of microfracture mechanics [21] but did not conduct in-depth research on the impact of internal stress evolution on the cyclic characteristics of the FGH96 superalloy. Therefore, the research on the evolution of internal stress during the cyclic process is helpful to further understand the cyclic deformation characteristics of the FGH96 superalloy and is very useful for the next step of constitutive modeling of the FGH96 superalloy. It is also of great significance for the safe application of the FGH96 superalloy in the key components of aero-engines.

2. Experimental Materials and Methods

2.1. Experimental Materials

The experimental material is the FGH96 powder metallurgy superalloy, which is powered by the plasma rotating electrode process (PREP) + hot isostatic pressing (HIP) to prepare disc blanks + isothermal forging. The specific heat treatment method is as follows: complete solid solution at 1110~1120 °C for 2 h, salt quenching at 600 °C, and heat preservation at 760 °C for 16 h, then air cooling after cooling to 550 °C in the furnace.

In this experiment, the FGH96 superalloy specimens were processed into cylindrical bars through an electrical discharge machining process. The main chemical composition of the FGH96 superalloy in this experiment is shown in Table 1. The specific dimensional parameters of the specimen are shown in Figure 1.

Table 1. Main element composition of the FGH96 superalloy specimen (wt./%).

Element	Ni	Cr	Co	W	Mo	Ti	Al
wt./%	Bal.	15.43	12.94	4.12	4.11	3.51	2.26

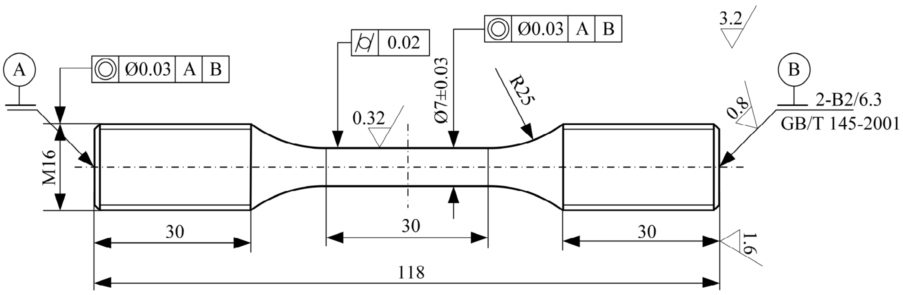

(**a**)

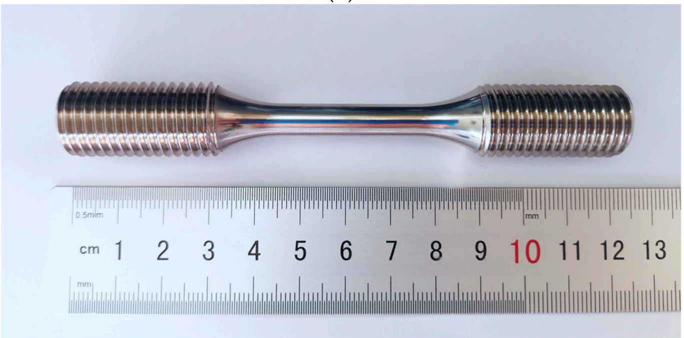

(**b**)

Figure 1. The FGH96 superalloy specimen: (**a**) geometries of specimen, data from [22] (unit: mm); (**b**) real specimen.

2.2. Fatigue Test Equipment and Method

The electro-hydraulic servo testing machine (MTS Systems Co., MTS-370.1, Eden Prairie, MN, USA) was used to carry out the strain-controlled high-temperature low-cycle fatigue tests, which is equipped with a high-temperature furnace system (MTS Systems Co., MTS 653, Eden Prairie, MN, USA) to ensure that the test temperature fluctuation does not exceed ±1 °C. Asbestos ropes were used to tie three K-type thermocouples to the upper, middle, and lower parts of the specimen to ensure that it was evenly heated. A push-type high-temperature axial extensometer (MTS Systems Co., MTS 632.53F-11, USA) was used to measure the axial deformation of the specimen in the low-cycle fatigue test, of which the gauge length is 25 mm. The extensometer was led out of the heating furnace through two ceramic rods. The equipment and the installation diagram of the specimen are shown in Figure 2.

The strain-controlled high-temperature low-cycle fatigue test was carried out with reference to the standard of GB/T 26077-2021, "Metallic Materials—Fatigue Test—Axial Strain Control Method" [23]. Referring to the service temperature of the high-pressure turbine disk key part of a certain type of aero-engine, a temperature of 550 °C was selected as the test temperature, which can better reflect the actual service conditions of the aero-engine high-pressure turbine disks. The triangular waveform with strain ratio $R = -1$ was selected for fatigue loading, and the strain rate was a fixed value of 0.005 s^{-1}. Four strain amplitudes $\varepsilon_a/2$ of 0.5%, 0.6%, 0.8%, and 1.2% were selected for low-cycle fatigue testing.

In order to ensure the reproducibility of the test results and meet the requirements of the standard [23], 8 fatigue tests were performed at each strain amplitude, and the average of these 8 tests was taken as the result of this group of tests. In order to eliminate errors in the test results caused by individual defective specimens, in accordance with the provisions of Standard [23], a pre-tension test was conducted before the formal loading of the test to determine whether the elastic modulus of the specimen met the error of ±5%. The specimen that does not meet this requirement will be eliminated, and a new specimen will be selected for re-testing. Since the pre-tension test in the standard is loaded in the micro-elastic range, it will not have a major impact on the low-cycle fatigue test results.

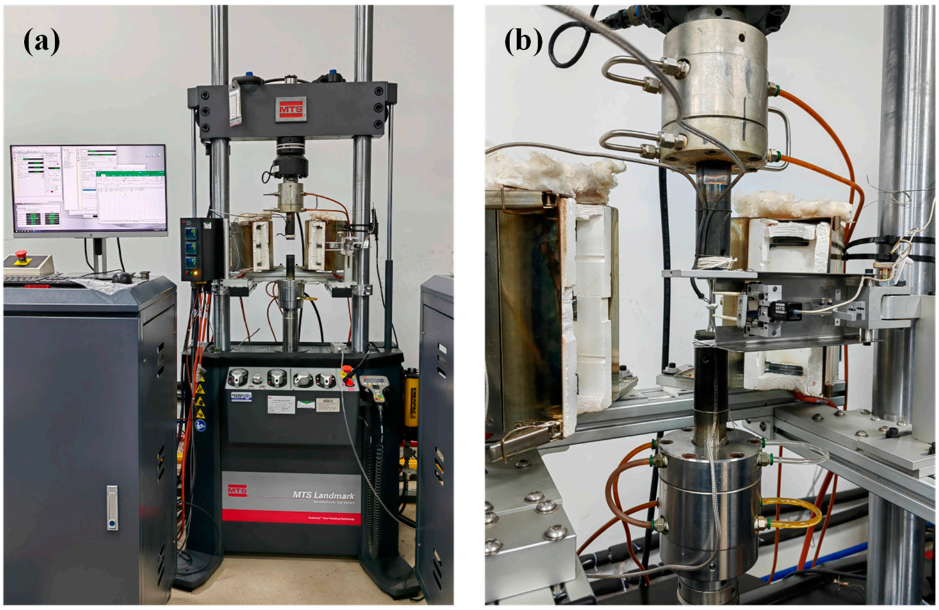

Figure 2. The testing equipment (**a**) and the installation diagram (**b**).

2.3. Cottrell's Internal Stress Division Method

According to the internal stress division theory proposed by Cottrell et al. [9], using the cyclic stress-strain hysteresis curve, the maximum stress under each cycle can be decomposed into back stress X, viscous stress σ_v, and isotropic stress Q. The viscous stress σ_v and the isotropic stress Q together constitute the effective stress σ_{eff}, which is as follows:

$$X = \frac{\sigma_e^{max} + \sigma_e^{min}}{2} \tag{1}$$

$$\sigma_v = \sigma_{max} - \sigma_e^{max} \tag{2}$$

$$Q = \frac{\sigma_e^{max} - \sigma_e^{min}}{2} \tag{3}$$

$$\sigma_{eff} = \sigma_v + Q \tag{4}$$

Among them, σ_e^{max} and σ_e^{min} respectively represent the maximum elastic stress and the minimum elastic stress of the linear elastic section in the hysteresis loop of the unloading section.

The key to this method is to determine the linear elastic part of the unloading section. To this end, the improved internal stress division method of Kuhlmann-Wilsdorf [24] was used to determine the linear elastic part by fitting the elastic modulus of the linear elastic section and introducing the plastic strain offset. The schematic diagram of the method is shown in Figure 3.

Considering that there is no dwell time at the peak stress under strain loading and the selected loading/unloading rate is not enough to produce obvious viscous stress, this paper does not distinguish viscous stress and isotropic stress separately and only selects back stress and effective stress as internal stress components for analysis. Based on the equipment accuracy and the fluctuation of sampling data, the value of ε_{off} was set to 5×10^{-5}.

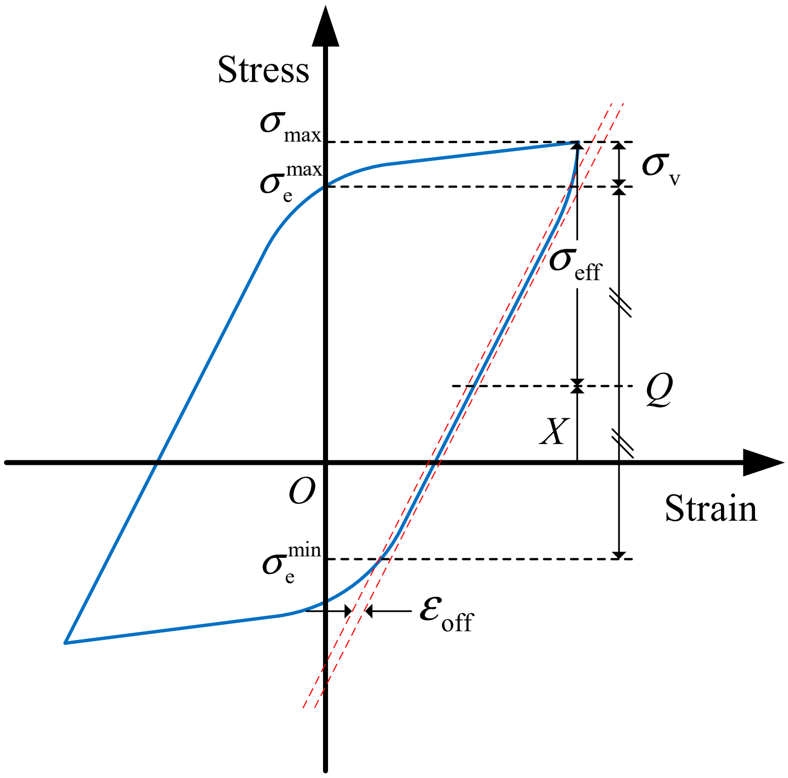

Figure 3. The division method of internal stress.

3. Results and Discussion

3.1. Cyclic Softening/Hardening Properties

The results of the high-temperature, low-cycle fatigue test are shown in Figure 4. The figure reflects the change of the peak stress σ_{max} of the FGH96 superalloy with the cycle count n under various strain amplitudes. It can be seen from Figure 4 that the FGH96 superalloy appears to have different cyclic softness/hardening characteristics under different strain amplitudes, especially in the early stages of cycles. When the strain amplitude is 0.5%, the FGH96 superalloy exhibits the characteristics of a slight softening-stable-softening fracture. When the strain amplitude is 0.6%, the FGH96 superalloy shows the characteristics of rapid hardening after a softening-stable-softening fracture. When the strain amplitude is between 0.8% and 1.2%, the FGH96 superalloy shows the characteristics of hardening–stabilization–softening fracture as a whole. A large number of experiments have shown that in the early stage of a high-temperature, low-cycle fatigue test, the material may be cyclically unstable due to the influence of the cyclic load and changes in the internal structure of the material. This phenomenon of initial cycle instability is common in powder metallurgy superalloys [25]. By comparing various curves, it can also be found that with the increase in strain amplitude, the peak stress σ_{max} in the stable section gradually increases, while the fatigue life shows a downward trend. In previous work [21], our research group carefully analyzed the different cyclic response characteristics of the FGH96 superalloy in the early cycles through the stress-strain hysteresis curves under various strain amplitudes. Next, the cyclic softening/hardening characteristics of the FGH96 superalloy in the early cycles will be analyzed from the perspective of the relationship between the half-life hysteresis curves and the uniaxial tensile curve.

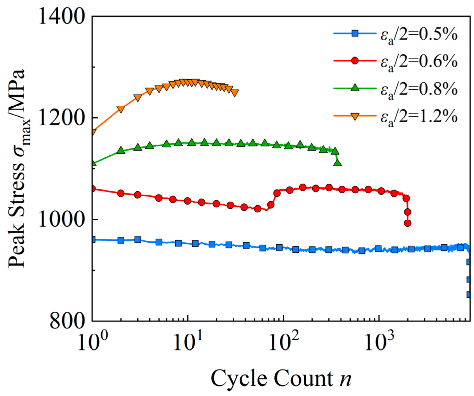

Figure 4. Peak stress response.

Figure 5 plots the half-life stress-strain hysteresis curves under the four strain amplitudes and the uniaxial tensile curve of the FGH96 superalloy at 550 °C. After enlarging the cyclic stress peak part, it can be seen that when the strain amplitude is lower than 0.6%, the stress peak of the half-life hysteresis curve is below the monotonic tensile curve, indicating that the FGH96 superalloy overall shows a cyclic softening trend in the early stage of cycling. When the strain amplitude is greater than 0.8%, the stress peaks are all above the uniaxial tensile curve, which reflects that the FGH96 superalloy mainly exhibits cyclic hardening in the early stages of cycles under high strain amplitude. Existing research shows that the cyclic softening or hardening of metallic materials mainly depends on the initial state [26], structural characteristics [27], strain amplitude, temperature [28], size effect [29], and other factors of the material. In other metallic materials [10,20,30,31], strain range-dependent characteristics similar to those of the FGH96 superalloy have also been found; that is, as the strain amplitude changes, the material exhibits different cyclic characteristics. Next, this characteristic of the FGH96 superalloy will be analyzed from the perspective of internal stress evolution.

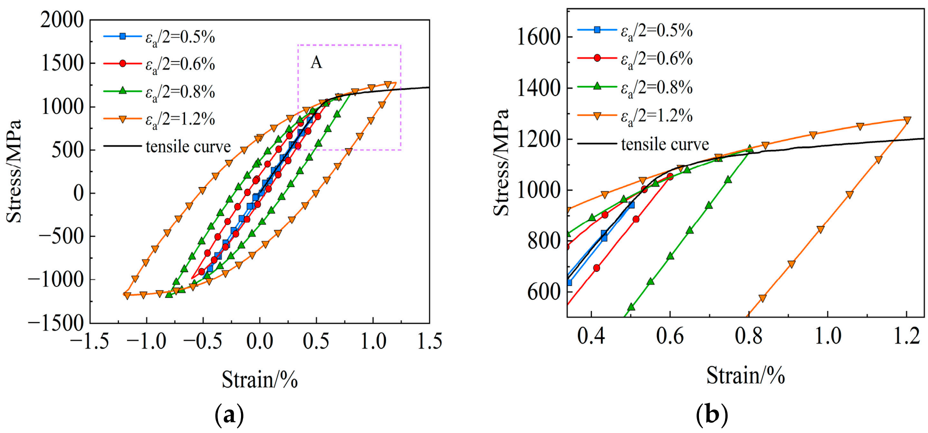

Figure 5. Half-life stress-strain hysteresis curves: (**a**) full curves; (**b**) enlarged view of area A.

3.2. Internal Stress Evolution

In order to obtain the evolution of each internal stress component of the FGH96 superalloy under cyclic loading, Cottrell's internal stress division method shown in Figure 3 was used to separate the internal stress of the stress-strain hysteresis loop under each cycle. Figure 6 shows the curves of back stress and effective stress with cycle number n at various strain amplitudes separated from the stress-strain hysteresis loop. It can be seen from the figure that, under all strain amplitudes, the magnitude of the effective stress is always greater than the back stress. Although the cyclic softening/hardening laws of the FGH96 superalloy are different under different strain amplitudes, the changing laws of back stress and effective stress under various strain amplitude cycles are basically similar. Similar to the cyclic softening/hardening behavior of the FGH96 superalloy, the evolution law of internal stress can also be divided into three obvious stages. In the early stages of the cycles, the back stress tends to harden, and the effective stress tends to soften. In the middle of the cycles, after the back stress and effective stress reach the saturation value, they maintain a stable state. At the end of the cycles, the back stress and effective stress soften until they fracture.

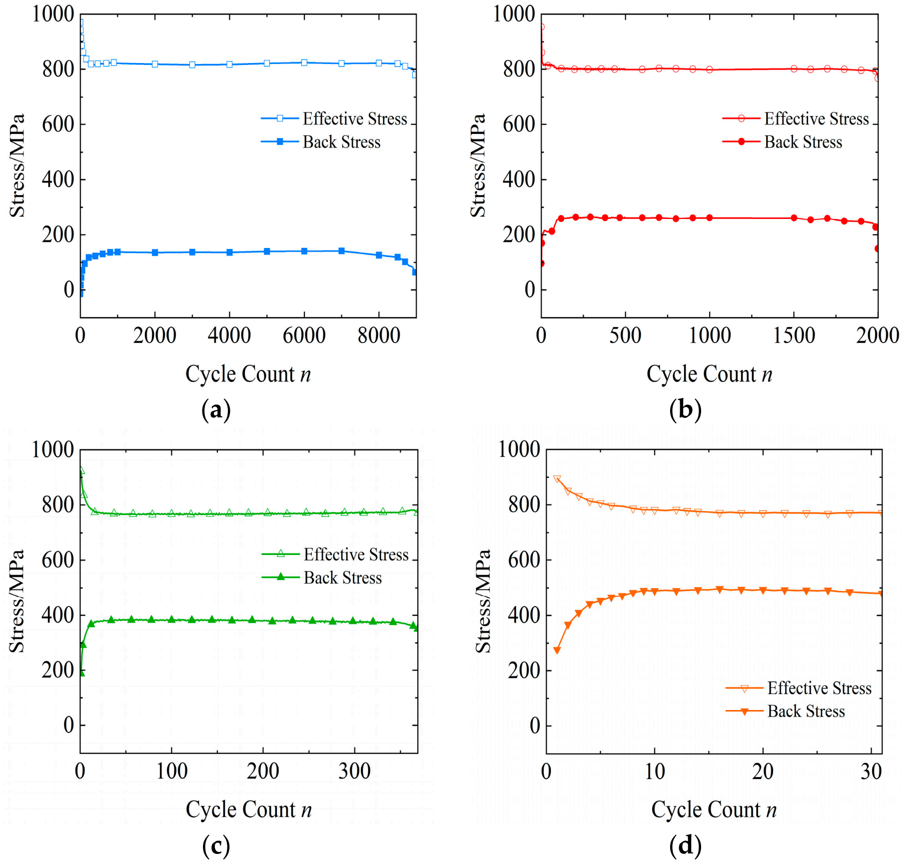

Figure 6. Evolution curves of back stress and effective stress: (**a**) $\varepsilon_a/2$ = 0.5%; (**b**) $\varepsilon_a/2$ = 0.6%; (**c**) $\varepsilon_a/2$ = 0.8%; (**d**) $\varepsilon_a/2$ = 1.2%.

Combined with the cyclic softening/hardening characteristics of the FGH96 superalloy in Section 3.1, it can be seen that the early evolution law of internal stress has a greater impact on the cyclic softening/hardening behavior of the FGH96 superalloy. In the study of the cyclic characteristics of the Ti-6Al-4V alloy, Xu [10] found that both back stress and effective stress affect its cyclic characteristics. The change pattern of the Ti-6Al-4V alloy in the early stages of the cycles is similar to that of the FGH96 superalloy. From this, it can be inferred that back stress and effective stress jointly affect the cyclic softening/hardening behavior of the FGH96 superalloy. In order to clarify the change law of internal stress with strain amplitude, the following discussion focuses on the change amount and stable value of internal stress in the early stages.

Figures 7 and 8 show the evolution of internal stress change value $\Delta\sigma$ and internal stress saturation value σ_s under different strain amplitudes in the early stage of the FGH96 superalloy cycles. Among them, the internal stress change value $\Delta\sigma$ is defined as the difference between the internal stress saturation value σ_s and the internal stress initial value σ_0, which is as follows:

$$\Delta\sigma = \sigma_s - \sigma_0 \tag{5}$$

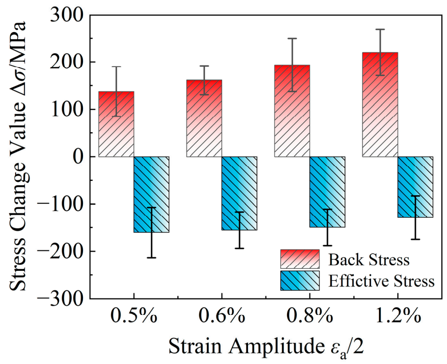

Figure 7. Internal stress change value in the early cycles.

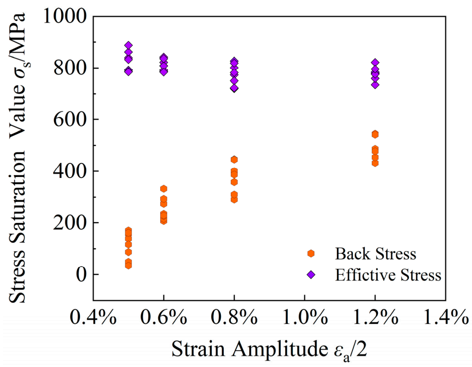

Figure 8. Internal stress saturation value in the middle cycles.

As can be seen from Figures 7 and 8, whether it is the internal stress change value or the internal stress saturation value, the back stress shows an obvious correlation with the strain amplitude. The larger the strain amplitude is, the larger the change value of back stress is, and the saturation value of back stress also increases obviously. In contrast, the change in effective stress is not significant. As the strain amplitude increases, although the saturation value and variation of the effective stress show a downward trend, the magnitude of the decrease is significantly weaker than the variation of the back stress. Since the saturation value of back stress increases significantly with the increase in strain amplitude, the steady-state value of the peak stress of the FGH96 superalloy in Figure 4 also increases with the increase in strain amplitude.

As can be seen from Figure 6, the number of cycles required for the back stress and effective stress to reach saturation values in the early stage for each strain amplitude is basically the same. Therefore, the change in internal stress in Figure 7 also reflects the speed of back stress increase/effective stress decrease. In addition, the sum of back stress and effective stress is the cyclic peak stress, according to the internal stress division theory. Therefore, it can be seen from the early evolution rate of the internal stress component reflected in Figure 7 that the cyclic softening/hardening behavior of the FGH96 superalloy in the early stages of cycles is the result of the competition between back stress hardening and effective stress softening. When the strain amplitude is low (0.5% and 0.6%), the hardening speed of the back stress is slightly lower than the softening speed of the effective stress. The effective stress softening contributes more to cyclic properties than the back stress hardening, so the FGH96 superalloy mainly exhibits cyclic softening characteristics in the early stages of the cycles. When the strain amplitude is high (0.8% and 1.2%), the hardening speed of the back stress is significantly higher than the softening speed of the effective stress. The contribution of the back stress to the cyclic characteristics is the main factor, and the FGH96 superalloy shows the characteristics of cyclic hardening in the early stage of the cycles under the corresponding strain amplitude. When Liang [16] and Yang [20] analyzed the cyclic softening and hardening of AISI 316L and 2.25CrMoV alloy, they also used the method of internal stress change to characterize their contribution to cyclic softening and hardening, explaining the cyclic softening and hardening characteristics of AISI 316L and 2.25CrMoV alloy. Based on this method, they also established the cyclic constitutive model and achieved good simulation accuracy. Considering that both the back stress and the effective stress shown in Figure 6 are softening in the late cycles, under the combined effect of the two, the FGH96 superalloy shows cyclic softening characteristics at the end of the cycles.

3.3. Microscopic Mechanism of Internal Stress Evolution

In the previous study, our research group explained the link between the microscopic fracture mechanism and the cyclic softening/hardening behavior of the FGH96 superalloy [21]. In this section, the micro-mechanisms summarized in the previous study will be combined to analyze the different properties exhibited by the FGH96 superalloy under different strain amplitudes from the perspective of internal stress evolution.

Existing research shows that whether a metal material undergoes cyclic softening or hardening depends on the initial state of the material, structural characteristics, strain amplitude, temperature, and other factors. At the same time, the cyclic softening/hardening phenomenon is closely related to dislocation motion [25,31,32]. When conducting scanning electron microscopy (SEM) observation of the fracture surface of the FGH96 superalloy specimen under cyclic loading, a large number of micro-cleavages composed of smooth facets can be seen in the rapid crack expansion area, as shown in Figure 9. The formation of micro-cleavage is related to the dislocation movement inside the FGH96 superalloy. Under the action of a low-cycle fatigue load, plastic deformation occurs inside the material, and dislocation slippage is caused. The continuous movement and aggregation of dislocations form micro-cleavage. Through transmission electron microscopy observations, Liu et al. [25] found that in the early stages of the cycles, dislocations gather around the γ' strengthening phase of the alloy. The dislocation density at the origin of the crack is relatively large and difficult to move, causing dislocation pile-up, which makes the dislocation density distribution uneven within the material and results in a dislocation density gradient. Back stresses are related to long-range interactions caused by local incompatibilities in plastic deformation [8]. As a result, the dislocation density gradient generates back stress. As the amplitude of the cyclic strain increases, the plastic strain produced by a single cycle increases, leading to the accelerated accumulation of plastic strain and deterioration of the internal organization of the material, manifested by deeper and longer secondary cracks. At the same time, the degree of dislocation pile-up increases and the dislocation density gradient increases, which leads to a rapid elevation of the back stress in the early cycles. Through transmission electron microscopy observations, Xu [10] and Liang [16] verified that the increase in dislocation density gradient is the cause of the increase in back stress in metal materials.

For effective stress, a large number of studies have shown that its change during cyclic loading is related to the short-range interaction of dislocations (such as interstitial atoms, precipitated particles, etc.), which is usually affected by the dislocation density within the material [13]. Pham and Holdsworth [33] found that the cross-slip enhancement leads to an increase in the annihilation rate of screw dislocations through the high-temperature cyclic tests of AISI 316L, which ultimately leads to a reduction in the density of dislocations. Based on the same softening behavior shown by the effective stress of AISI 316L in the early stage under high-temperature cyclic loading, it can be speculated that the FGH96 superalloy is affected by cross-slip enhancement in the early stage of the cycle, and the effective stress shows a softening trend due to the reduction in dislocation density.

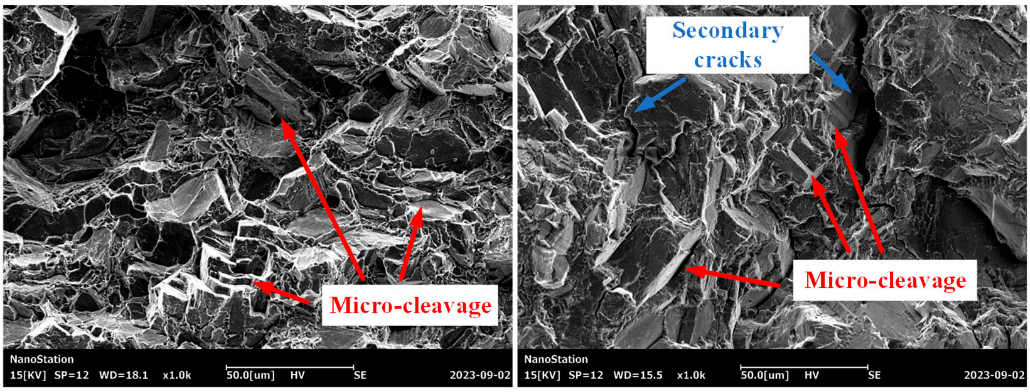

(**a**) (**b**)

Figure 9. Morphology of the rapid crack expansion zone of specimen fracture: (**a**) $\varepsilon_a/2 = 0.6\%$; (**b**) $\varepsilon_a/2 = 1.2\%$.

4. Conclusions

In this paper, the strain-controlled high-temperature low-cycle fatigue behavior of the FGH96 superalloy was analyzed by Cottrell's internal stress division theory. According to the evolution law of back stress and effective stress under different strain amplitudes, the reasons for different cyclic softening/hardening in the early stages of the cycles of the FGH96 superalloy are explained. Throughout the work of this paper, the conclusions are as follows:

(1) The different cyclic softening/hardening characteristics of the FGH96 superalloy under different strain amplitudes are closely related to the evolution of internal stress.
(2) During the entire cycle, the back stress shows a hardening trend in the early stage, and the effective stress mainly shows a softening trend. The magnitude of the strain amplitude has a great influence on the back stress of the FGH96 superalloy, but the effect on the effective stress is not significant.
(3) In the early cycle, affected by the competition between back stress hardening and effective stress softening, the FGH96 superalloy exhibits different cyclic softening/hardening characteristics under different strain amplitudes. In the late cycles, affected by the joint softening of back stress and effective stress, the FGH96 superalloy shows cyclic softening characteristics at all strain amplitudes.
(4) The dislocation density gradient caused by dislocation accumulation leads to the rapid increase of the FGH96 superalloy's back stress at high strain amplitude in the early cycles. The reduction in the effective stress of the FGH96 superalloy is due to the reduction in dislocation density caused by the enhanced cross-slip.

Author Contributions: Conceptualization and writing—original draft preparation, Z.L.; methodology and formal analysis, Z.L., H.Q., K.X. and Z.X.; supervision and writing—review and editing, H.Q., K.X. and Z.X.; data curation, H.Q. and Z.X.; investigation, validation, and visualization, P.J. and M.J. All authors have read and agreed to the published version of the manuscript.

Funding: This research received no external funding.

Data Availability Statement: The data presented in this study are available on request from the corresponding author.

Conflicts of Interest: The authors declare no conflict of interest.

References

1. Bai, Y.; Yang, S.; Zhu, M.; Fan, C. Study on Microstructure and Fatigue Properties of FGH96 Nickel-Based Superalloy. *Materials* **2021**, *14*, 6298. [CrossRef] [PubMed]
2. Wang, R.; Gu, H.; Liu, Y.; Miura, H.; Zhang, X.-C.; Tu, S.-T. Surrogate-modeling-assisted creep-fatigue reliability assessment in a low-pressure turbine disc considering multi-source uncertainty. *Reliab. Eng. Syst. Safety* **2023**, *240*, 109550. [CrossRef]

3. Zhao, X.; Wang, Z.; Lv, J.; Liu, X.; Zheng, L.; Liu, J. Oxidation Property of a Fourth-Generation Powder Metallurgy FGH4108 Nickel-Based Superalloy. *Metals* **2023**, *13*, 945. [CrossRef]
4. Liu, A.; Zhang, Y.T.; Wang, X.S.; Xu, W.; Zhang, Y.; He, Y.H. Evaluation of the influences of the stress ratio, temperatures, and local microstructure on small fatigue crack propagation behavior of the FGH96 superalloy. *Int. J. Fatigue* **2023**, *171*, 107573. [CrossRef]
5. Li, L.; Liu, F.; Nie, S.; Wang, Q.; Zhao, R.; Zhang, Y.; Feng, H.; Lin, X. Effect of Thermal Cycling on Grain Evolution and Micro-Segregation in Selective Laser Melting of FGH96 Superalloy. *Metals* **2023**, *13*, 121. [CrossRef]
6. Wang, H.; Zhang, J.; Shang, H.; Sha, A.; Cheng, Y.; Duan, H. Experiment and Modelling of the Pre-Strain Effect on the Creep Behaviour of P/M Ni-Based Superalloy FGH96. *Materials* **2023**, *16*, 3874. [CrossRef] [PubMed]
7. Kong, W.; Wang, Y.; Chen, Y.; Liu, X.; Yuan, C. Investigation of uniaxial ratcheting fatigue behaviours and fracture mechanism of GH742 superalloy at 923 K. *Mater. Sci. Eng. A* **2022**, *831*, 142173. [CrossRef]
8. Xuan, F.; Zhao, P. *Cyclic Viscoplasticity Behaviour and Constitutive Theory of High Temperature Structures*; Science Press: Beijing, China, 2021; p. 55.
9. Cottrell, A. *Dislocations and Plastic Flow in Cristals*; Oxford University Press: London, UK, 1953; Volume 111.
10. Xu, H.; Ye, D.; Mei, L. A study of the back stress and the friction stress behaviors of Ti-6Al-4V alloy during low cycle fatigue at room temperature. *Mater. Sci. Eng. A* **2017**, *700*, 530–539. [CrossRef]
11. Zhao, P.; Xuan, F.-Z.; Wu, D.-L. Cyclic softening behaviors of modified 9–12%Cr steel under different loading modes: Role of loading levels. *Int. J. Mech. Sci.* **2017**, *131–132*, 278–285. [CrossRef]
12. Zhang, Y.; Yang, C.; Zhou, D.; Zhe, Y.; Meng, L.; Zhu, X.; Zhang, D. Effect of stacking fault energy on microstructural feature and back stress hardening in Cu-Al alloys subjected to surface mechanical attrition treatment. *Mater. Sci. Eng. A* **2019**, *740–741*, 235–242. [CrossRef]
13. Wang, N.; Yu, H.; Zhao, P.; Zhang, J.-M.; Gong, J.-G.; Xuan, F.-Z. Cyclic deformation response of austenitic Ni-based alloy: Mechanical behavior, internal stress evolution and microstructural feature. *Mater. Sci. Eng. A* **2022**, *850*, 143522. [CrossRef]
14. Yin, P.; Zhang, W.; Zhang, Y.; Yang, Q.; Liang, F.; Chang, L.; Zhou, C. Cyclic deformation mechanism and fracture behaviour of 316L stainless steel under thermomechanical fatigue loading. *J. Mater. Res. Technol.* **2023**, *24*, 4484–4499. [CrossRef]
15. Zheng, X.T.; Wu, K.W.; Wang, W.; Yu, J.Y.; Xu, J.M.; Ma, L.W. Low cycle fatigue and ratcheting behavior of 35CrMo structural steel at elevated temperature. *Nucl. Eng. Des.* **2017**, *314*, 285–292. [CrossRef]
16. Liang, F.; Zhang, W.; Chen, F.; Yin, P.; Yang, Q.; Chang, L.; Zhou, C. Experimental and constitutive modelling studies of type 316L stainless steel based on internal stress under low cycle fatigue and creep-fatigue interaction. *Int. J. Fatigue* **2023**, *175*. [CrossRef]
17. Wang, C.; Xuan, F.-Z.; Zhao, P.; Guo, S.-J. Effect of cyclic loadings on stress relaxation behaviors of 9–12%Cr steel at high temperature. *Mech. Mater.* **2021**, *156*, 103787. [CrossRef]
18. Xu, L.-Y.; Fan, J.-S.; Yang, Y.; Tao, M.-X.; Tang, Z.-Y. An improved elasto-plastic constitutive model for the exquisite description of stress-strain hysteresis loops with cyclic hardening and softening effects. *Mech. Mater.* **2020**, *150*, 103590. [CrossRef]
19. Zhong, Y.-L.; Wang, Y.-B.; Xiang, Y.; Li, G.-Q. Constitutive model for cyclic behavior of mild steel under various strain amplitudes. *J. Constr. Steel Res.* **2022**, *196*, 107396. [CrossRef]
20. Yang, Q.; Zhang, W.; Guo, Y.; Liang, F.; Yin, P.; Chang, L.; Zhou, C. A universal constitutive model considering strain range dependence effect and transient behaviour for both cyclic softening and hardening steels. *Eng. Fract. Mech.* **2023**, *290*, 109481. [CrossRef]
21. Li, Z.; Qin, H.; Xu, K.; Xie, Z.; Ji, P.; Jia, M. Fatigue Behavior of the FGH96 Superalloy under High-Temperature Cyclic Loading. *Materials* **2023**, *16*, 5883. [CrossRef]
22. *GB/T 145-2001*; Center Holes. Standardization Administration of the People's Republic of China (SAC): Beijing, China, 2001.
23. *GB/T 26077-2021*; Metallic Materials—Fatigue Testing—Axial-Strain-Controlled Method. Standardization Administration of the People's Republic of China (SAC): Beijing, China, 2021.
24. Kuhlmann-Wilsdorf, D.; Laird, C. Dislocation behavior in fatigue II. Friction stress and back stress as inferred from an analysis of hysteresis loops. *Mater. Sci. Eng.* **1979**, *37*, 111–120. [CrossRef]
25. Liu, X.; Tao, C.; Feng, Y. *Damage Behavior and Life Prediction of Powder Metallurgy Superalloys*; Aviation Industry Press: Beijing, China, 2018; p. 34.
26. Abedi, H.R.; Hanzaki, A.Z.; Azami, M.; Kahnooji, M.; Rahmatabadi, D. The high temperature flow behavior of additively manufactured Inconel 625 superalloy. *Mater. Res. Express* **2019**, *6*, 116514. [CrossRef]
27. Guo, Q.; Hou, H.; Pan, Y.; Pei, X.; Song, Z.; Liaw, P.K.; Zhao, Y. Hardening-softening of Al0.3CoCrFeNi high-entropy alloy under nanoindentation. *Mater. Des.* **2023**, *231*, 112050. [CrossRef]
28. Guo, G.; Ding, C. *Mechanical Testing of Aeronautical Materials*; China Machine Press: Beijing, China, 2020; p. 241.
29. Niu, X.; Zhu, S.; He, J. Defect tolerant fatigue assessment of AM materials: Size effect and probabilistic prospects. *Int. J. Fatigue* **2022**, *160*, 106884. [CrossRef]
30. Cao, W.; Yang, J.; Zhang, H. Unified constitutive modeling of Haynes 230 including cyclic hardening/softening and dynamic strain aging under isothermal low-cycle fatigue and fatigue-creep loads. *Int. J. Plast.* **2021**, *138*, 102922. [CrossRef]
31. Nguyen, T.; Yoon, K.; Park, J.; Baek, U. Characterization of Strain-Controlled Low-Cycle fatigue and fracture behavior of P91 steel at elevated temperatures. *Eng. Fail. Anal.* **2022**, *133*, 105887. [CrossRef]

32. Li, B.; Yang, J.; Wang, Z.; Chen, G.; Chen, X. Low cycle fatigue behavior of 316LN stainless steel: Effects of temperature, strain rate and strain amplitude. *Int. J. Fatigue* **2023**, *175*, 107767. [CrossRef]
33. Pham, M.-S.; Holdsworth, S.R. Evolution of Relationships Between Dislocation Microstructures and Internal Stresses of AISI 316 L During Cyclic Loading at 293 K and 573 K (20 °C and 300 °C). *Metall. Mater. Trans. A* **2014**, *45*, 738–751. [CrossRef]